Check for updates

Superhydrophobic foam combined with biomass-derived TENG based on upcycled coconut husk for efficient oil–water separation†

Jiaming Liang, [iD] Yajuan Zhou, [iD] Qian Wu, [iD] Zeying Zhu, [iD] Keda Lin, [iD] Jinsheng He, [iD] Haihe Hong [iD] and Yuanzheng Luo [iD] *

The ocean ecological environments are seriously affected by oil spilling and plastic-debris, preventing and significantly reducing marine pollution *via* using biocomposite production from natural fiber reinforcement is a more friendly way to deal with marine oil pollution. Herein, we upcycled coir-coconut into lignin and coconut shell into spherical TENG by a combination of dip-dry and chemical treatment and used the SiO_2 nanoparticles together with cellulose nanofibrils to prepare serial sugar-templated, anisotropic and hybrid foams. The as-prepared lignin/SiO_2 porous sponge (LSPS) with a hierarchical porous morphology and uniformly dispersed nanoparticles structure benefits from the advantages of biomass-based additives, which presents reversible large-strain deformation (50%) and high compressive strength (11.42 kpa). Notably, the LSPS was significantly more hydrophobic (WCA ≈150°) than pure silicone-based foams, and its selective absorbability can separate oil from water under continuous pumping. Meanwhile, the coconut husk was also upcycled as a spherical TENG shell by a combination of the nanofiber-enhanced polymer spherical oscillator (CESO), which possessed high triboelectric properties (U_{oc} = 272 V, I_{sc} = 14.5 μA, Q = 70 nC) and was comparable to the plastic shell TENG at low frequency (1.6 Hz). The monolithic foam structure developed using this clean synthetic strategy holds considerable promise for new applications in sustainable petroleum contamination remediation.

1 Introduction

Plastic and petroleum (oil) pollution are both recognized as severe anthropogenic issues in marine and coastal ecosystems worldwide, which have arisen in a few decades and are increasing rapidly.[1–3] Therefore, separating oil and plastic pollutants from water bodies has attracted particular attention over the years. Among the environmental remediation strategies for oil spills, mechanical remediation using sorbent materials is considered one of the most efficient and cost-effective methods.[4] Up to now, various sorbent materials with different surface morphology and porous structures capable of removing the spilled oil/solvents from wastewater, such as natural-based hydrophilic monolith, inorganic mineral products, polymeric sponges, and carbon-based nanomaterials. Due to their high accessible pore volume, unique wettability, and modification possibilities, the foamed and natural-derived materials have obvious advantages over other absorbents.

Depending upon the geological position, searching for an effective, inexpensive, and readily available adsorbent material

that exhibits excellent surface properties is necessary. In this sense, various agricultural waste materials are the most promising and renewable source of adsorbent materials in tropical coastal areas. The coconut husk (CH), as a renewable natural polymer, contains about 38% lignin,[5] which has a rigid structure of benzene ring,[6,7] and it is rich in hydroxyl groups, which is conducive to the grafting modification of chemicals on lignin.[8] There has been a growing interest in developing various lignin-based adsorbents for its eco-friendliness, low toxicity, biocompatibility, and lipophilicity.[9–14] Haodong Sun *et al.*[8] developed a superhydrophobic porous material named SHP-MRSs (superhydrophobic melamine resin sponges) composed of lignin, HDTMS (hexadecyltrimethoxysilane) and melamine resin sponge *via* simple impregnation. The oil–water separation efficiency of SHP-MRSs was up to 98.6%, and the SHP-MRSs remained superhydrophobic after multiple separation cycles. Yi Meng *et al.*[10] neutralized and aminated lignin with AA (acrylic acid) and GO (graphene oxide), prepared LHGO (lignin-based hydrogel enhanced by graphene oxide) with mixed solution, and then annealed the hydrogel to prepare LCAGO (lignin-based carbon aerogel enhanced by graphene oxide) for oil–water separation. At 350 °C, the WCA (water contact angle) of LCAGO can reach 150° and maintain for 2 hours. Xiaoyu Gong *et al.*[15] used acetonitrile extraction TL (technology lignin) to disperse more phenolic hydroxyl, carboxyl and narrow molecular weight in TL, thereby

School of Electronic and Information Engineering, Guangdong Ocean University, Zhanjiang 524088, China. E-mail: luoyz@gdou.edu.cn

improving the binding strength with filter paper and nano-SiO$_2$. A stable micro-nano binary structure was formed on the surface of filter paper as the hydrophobic to develop AEL-FP (acetonitrile extracted lignin-based paper composite). The oil–water separation efficiency of AEL-FP can reach 98.6%, and the WCA is 168°. With regard to lignin extracted from coconut shell, Zhu Wan-Ying et al.[5] successfully extracted lignin from coconut shell fiber with ionic liquid [Bmin]HSO$_4$ (1-butyl-3-methylimidazole bisulfate) assisted by ethylene glycol under microwave heating conditions. Although various super-wettable materials are being developed to better separate oil from contaminated water, sorbent materials must be engineered to a scalable, rapid, continuous oil skimming with water pumps under actual sea conditions.

Conventionally powered pumps for widespread oil–water separation, such as diesel and electric pumps, require readily available electricity or fuels, which is hard to achieve under offshore conditions consistently. Therefore, it is necessary to design and develop an oil–water separation device with sustainable supplies of self-powered energy. Up to now, Profs Zhong Lin Wang[16] reported that novel spherical triboelectric nanogenerators (TENGs) have the potential for harvesting large-scale blue energy, which is more flexible, lightweight, cost-effective, and supposed to function in all weather conditions. The spherical friction nanogenerator can collect the omnidirectional wave energy through the omnidirectional friction between the internal polymer oscillator and Kapton film, and convert it into electric energy efficiently. Li et al. proposed a new spherical TENG based on the coupling of spring-assisted structure and swing structure, which was constructed to scavenge water wave energy.[17–19] Liu designed a spherical triboelectric nanogenerator (TENG) with two spring-like multilayer spiral units (MH-TENG) that utilize a charge-shuttle mechanism to collect water wave energy, providing a new strategy for smart marine sensing.[20] From this perspective, TENG can be applied to the oil–water separation pumping device for marine pollution control, collecting wave energy on the sea surface and purifying the seawater in real-time. Although spherical TENG can efficiently solve the problem of long-distance continuous power supply through in situ power generation, most of the current TENG uses plastic as the shell and bracing structure, which is non-degradable and easy to cause secondary plastic pollution to the environment. Inspired by this, the low-density coconut husk can replace TENG's plastic structure, which gives TENG unique properties such as biodegradability and floatability over the sea.

Herein, we propose a method of high hydrophobic foam and biomass-derived TENG based on upcycled coconut husk for efficient oil–water separation and a marine self-healing device combining biomass (Fig. 1a). In order to study the effect of lignin contained in coconut shell, we use ready-made alkali lignin to replace the study of coconut shell lignin. Firstly, the porous sponge mixed with PDMS and Ecoflex is prepared by sugar-added square template method, and then the porous sponge is put into acetonitrile, alkali lignin purified from ethanol and petroleum ether mixed with SiO$_2$ under ultrasonic condition. Lignin/SiO$_2$ porous sponge (LSPS) is prepared. The compressibility, compression recovery, water contact angle (WCA), oil contact angle (OCA), oil absorption mass and oil–

water separation capacity of LSPS are studied. We use ready-made nanocrystal-cellulose (CNC) to replace the cellulose in the coconut shell. By using the sugar ball template method, Ecoflex porous spherical vibrator fused with CNC is fabricated. Using the shell of waste coconut shell instead of acrylic ball shell as the shell of spherical friction nanogenerator, the biomass TENG—CNC/E-TENG is produced. To study the role of cellulose in TENG, we study the output current of CNC/E-TENG, as well as the durability of CNC/E (CNC was mixed with Ecoflex) by studying its stretchability in the form of thin films.

2 Experimental

2.1 Materials and instrumentation

Cellulose nanocrystals (CNC) were obtained from ScienceK (http://sciencek.com/). Ecoflex®00-30 silicone rubber Shole00-30 hardness was purchased from Smooth-On (https://www.smooth-on.com/). The liquid PDMS precursor was provided by Shanghai Angwei Technology Co., LTD. Kapton (width 10 mm) films were purchased from Shenzhen Xinhongsen Technology Co., LTD. And alkali lignin was obtained from Riococo Co., LTD, and stored at 15 °C before its application. Petroleum ether (AR, 90–120), n-heptane (AR), and other organic solvents were purchased from Guangdong HP Chemical Raw Material Reagent Co., LTD. nano-SiO$_2$ (oleophilic and hydrophobic type, 20 nm) were purchased from Banrui New Material Technology Co., LTD, and was ultrasonically cleaned and dried with alcohol before use. Aluminum films, sugar, coconut shells, molds and lightweight iron balls are all purchased from local supermarkets. Unless otherwise specified, all reagents and materials are used by accepted standards.

2.2 Preparation of the CESO and EPPS

The manufacturing procedure of the CNC/E spherical oscillators (CESO) is demonstrated in Fig. 2b. First, the spherical sugar mold was made by fulfilling the fine-granulated sugar in a rubber hollow ball, in which the spherical shell mold was sprayed with rubber mold releasing agent. Then, Ecoflex A, Ecoflex B, and CNC were mixed at 1:1:0.1 radio. And after pouring it straightly into the hollow mold, it was placed in a vacuum oven for about 45 minutes, to fully exhaust the air bubbles. Subsequently, it was heated at 120 °C for 4 h to solidify the mixture. Finally, the resultant was soaked in water for 1 h to dissolve the sugar particles in water to get the CESO.

The material ratio method was changed to Ecoflex A, and Ecoflex B, PDMS and Curing Agent were mixed at 1:1:1:0.1 radio. The E/P (Ecoflex is mixed with PDMS) porous sponge (EPPS) can be obtained by replacing the spherical mold with a cylindrical mold in the same manner as CESO, as shown in Fig. 2c. Furthermore, the compact EPPS can withstand reasonable handling and machining without collapse.

2.3 Preparation and processing mechanism of the EPSS and LSPS

As shown in Fig. 1c, 25 g alkali lignin was stirred in 250 ml acetonitrile by a magnetic mixer for 2 hours, and then
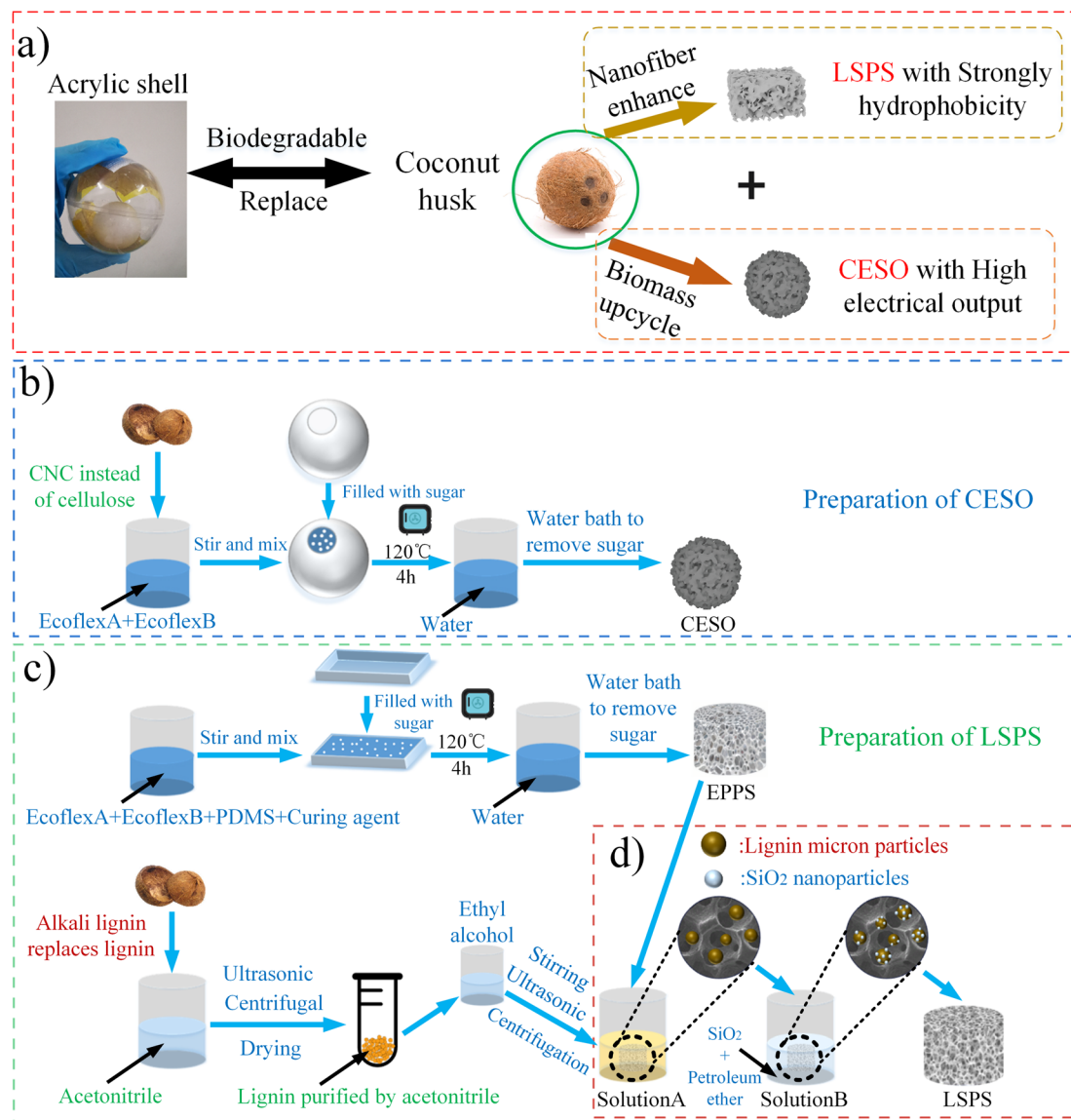
Fig. 1 (a) Schematic diagram of reuse of waste coconut shell waste. (b) Preparation of making CNC/E internal porous vibrator. (c and d) Preparation technology and mechanism of lignin/SiO$_2$ porous sponge.

ultrasonic was performed for 15 minutes. Straightly, the solid–liquid mixture was centrifuged at 8500 rpm for 10 minutes. Subsequently, the solution in the centrifuge tube was poured out to retain the insoluble part. ALA (Alkali-lignin modified by acetonitrile) was obtained by drying the insoluble fraction at 60 °C for 6 hours. Next, 2 g ALA was added to 22 ml ethanol, stirred for 1 hour and sonicated for 15 minutes, and the above operations were repeated more than 3 times. Then, a uniform solution, solution A, was obtained by centrifugation at 8500 rpm. Subsequently, solution B was obtained by adding 0.4 g of nano-SiO$_2$ to 40 ml of petroleum ether solvent and cyclically ultrasonic 3 times for 15 minutes (Fig. S1†). EPPS was immersed in solution A for 10 minutes with ultrasound. Then, it was soaked in solution B for another 30 minutes with ultrasound. After drying in an oven at 90 °C for 1.5 hours according to the dip-dry method,[21] LSPS can be

obtained. The above operations are shown in Fig. 1c and d. In the above operation, EPSS (SiO$_2$ porous sponge) can be produced by only reducing the steps of immersion in solution A.

As shown in Fig. 1d, acetonitrile reacts with alkali lignin. The cyanide group (–CN) of acetonitrile replaces the hydrophilic phenol group (OH) of alkali lignin, and removes impurities, pigments and other impure substances in the alkali lignin, thus obtaining lignin purified by acetonitrile. EPPS itself has a certain lipophilicity. When immersed in clear liquid A, the lipophilicity of the sponge enables it to adsorb lignin molecules dissolved in ethanol. Similarly, because lignin molecules are also oleophilic, it can further strengthen the adsorption force of the sponge on the mixture of petroleum ether and hydrophobic nano-SiO$_2$, so that the hydrophobic nano-SiO$_2$ is fixed on the sponge, and according to the principle of the dip-dry method,
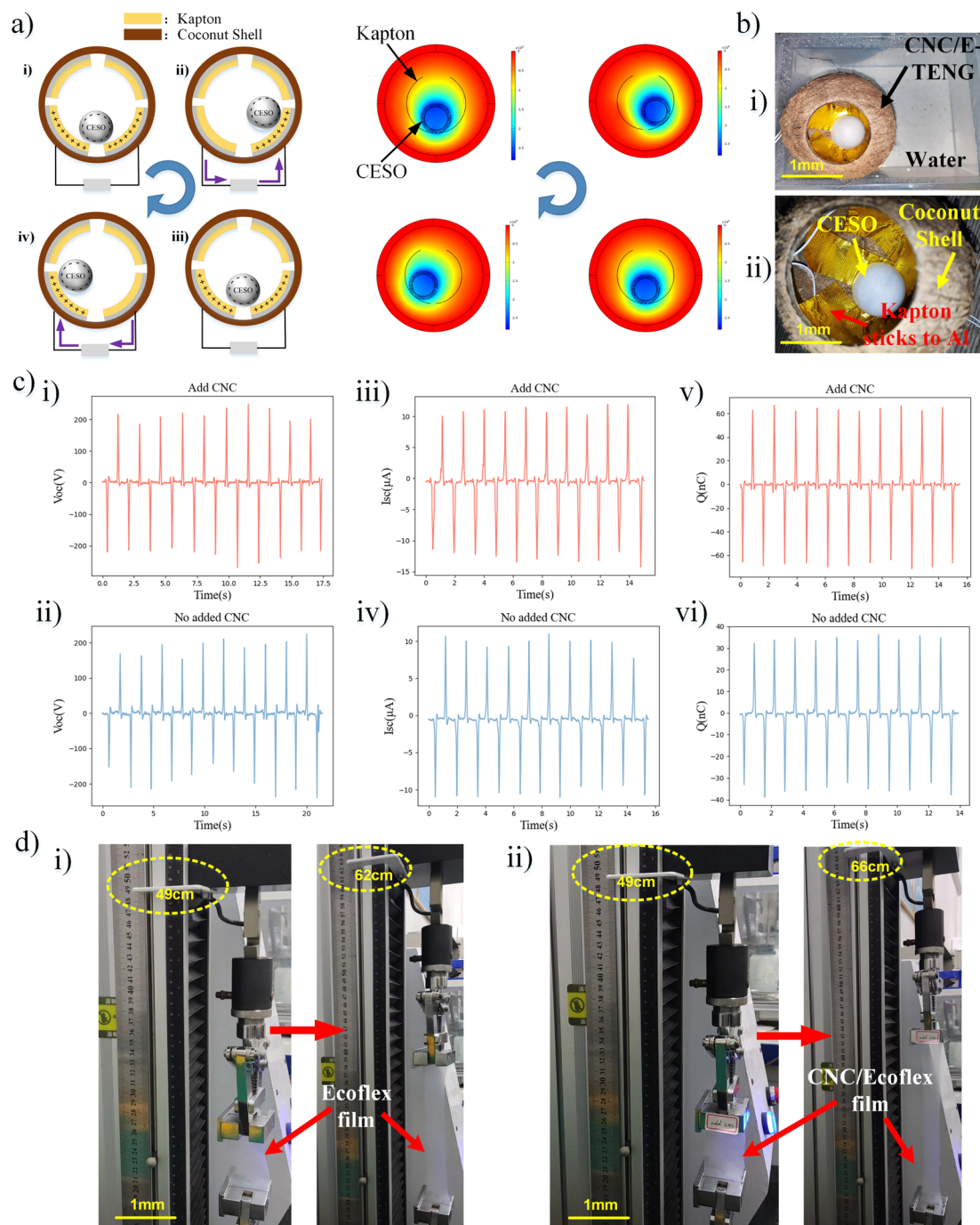
Fig. 2 (a) Spherical friction nanopower generation schematic diagram and comsol simulation. (b) Physical display and internal structure of CNC/E-TENG. (c) Electrical performance test. (d) Tensile strength graphs of Ecoflex film and CNC/Ecoflex film.

the oleophilic and hydrophobic material can be left in the EPPS to form an oleophilic and hydrophobic layer.

2.4 Preparation and principle of the CNC/E-TENG

A CNC/E-TENG can be obtained by combining a CESO with a coconut shell coated with a friction layer, which was assembled by core–shell structure in our preview work.[22] For detail, apply a layer of aluminum film to the inner surface of the coconut shell, and then apply Kapton to the surface of the

aluminum film. Finally, the CESO is placed in it, and an eco-friendly adhesive is used to incorporate the sliced coconut shell.

The power generation principle of the CNC/E TENG is demonstrated in Fig. 2a. The CESO and Kapton/Al electrodes with different polarities produce an equal amount of dissimilar friction charge on the surface after several contacts. Assuming the position in Fig. 2a(i) as the starting position, it can be seen that from the charge conservation, the charge amount of the CESO is equal to the sum of the Kapton charge amount of the

following two pieces. The potential difference between these two electrodes is zero, thus the external circuit has no current. When the CESO rolls to the position shown in Fig. 2a(ii), the charge flows from the left electrode to the right electrode through the external circuit by electrostatic induction. When the CESO moves to the position shown in Fig. 2a(iii), the charge flows from the right electrode to the left electrode through the external circuit. When the CESO is shown in Fig. 2a(iv), the charge flows from the right electrode to the left electrode through the external circuit. Thus, the mechanical energy generated by the wave is converted into electrical energy, and the alternating current is formed.[23] The right side of Fig. 2a shows the comsol simulation diagram of CNC/E-TENG, reflecting the voltage changes with the CESO rolling direction.

2.5 Characterization

An electrostatic detector (Keithley 6514) was used to measure the short circuit current of the CNC/E-TENG and the E-TENG. Using universal material testing machine, tensile control mode and tensile strain rate of 100%, to measure the tensile property of the material. Using universal material testing machine, compact model, the change of Young's modulus of LSPS was measured. Use an electronic scale (brand) to measure the mass of the object. Static contact Angle (CAs) was measured with DSA30 droplet shape analyzer. The sponge surface properties were observed by SEM. The X-ray diffraction (XRD) measurements were carried out using an X-ray source of CuKa radiation (X'Pert PRO DY2198) and were performed at a generator voltage of 40 kV and current of 40 mA, with a sweep angle (2°) from 5° to 60° at a rate of 2° per minutes. Infrared spectra were recorded using a Nicolet 6700 Fourier transform infrared (FTIR) spectroscope. Digital photos are obtained by a smartphone's camera mode.

2.6 Sponge oil absorption ratio measurement

The oil absorption capacity of a sponge is determined by the change in the weight of a sponge at room temperature until the sponge is saturated with liquid. Oil absorption capacity (Q_{oil}) is calculated based on the following equation values (1):

$$Q_{oil} = \frac{m_s - m_0}{m_0} \times 100\% \tag{1}$$

where m_0 is the mass before sponge adsorption, m_s is the mass after sponge adsorption. The absorption capacity of n-heptane, pump oil and soybean oil was measured respectively. Regarding viscosity: n-heptane < soybean oil < pump oil.

2.7 Sponge selective absorption and water–oil separation experiment

The selective adsorption of n-heptane floating on the water surface was carried out by LSPS using Sudan red II (AR) stained n-heptane solution to simulate the oil pollution on the sea surface. The position of the sponge was manually controlled during absorption. In addition, we further evaluated the durability of LSPS by recording the oil absorption rate of LSPS after 100 static suction/discharge cycles of n-heptane.

One end of the cylindrical LSPS sample was immersed in oil-covered water, while the inlet tube of the peristaltic pump was placed at the other end. A magnetic stirrer-rod is used to stir the water to simulate ocean conditions, stirring it into a rotating vortex with bubbles flowing upward. When the pressure drive system works, capillary action and selective absorption work together, and oil is extracted rapidly upward through the pipe. Therefore, the selective and efficient oil suction system can continuously extract the oil in the liquid through the tubing to the peristaltic pump and discharge the oil into the collection beaker. In the case of continuous pumping for a long time, the stable water level in the beaker indicates that the water is not removed by the LSPS.

LSPS conducted 20 dynamic oil–water separation experiments on n-heptane under different cycles. Replace the n-heptane of the same volume as the initial volume every five cycles (20 ml is used in this paper), and record the oil collected after oil–water separation under this cycle. Finally, combined with the volume of the initial oil, the oil–water separation efficiency of the sponge after every five cycles can be calculated. The tube diameter of the oil pump used in this experiment is 0.3 cm, and the maximum power is 5 W. The oil dialysis capacity of the LSPS under different cycles can be calculated by recording the time of oil–water separation.

3 Results and discussion

3.1 Electromechanical properties of CNC/E-TENG and E-TENG

Fig. 2b(i and ii) show photos of CNC/E-TENG device packaged in a coconut shell. As shown in Fig. 2c, open-circuit voltage, the short-circuit current and surface charge are generated by the friction between the oscillator and Kapton. Fig. 2c(i, iii and v) shows the open-circuit voltage (U_{oc}), short-circuit current (I_{sc}), and surface charge (Q) waveforms of the CNC/E-TENG with CESO, respectively. Fig. 2c(ii, iv and vi) shows the U_{oc}, I_{sc} and Q waveforms of E-TENG with a spherical Ecoflex oscillator without CNC (1.6 Hz). As shown in Fig. 2c(i and ii), the peak open-circuit voltage (U_{oc}) generated by CESO as an oscillator is 272 V. The peak U_{oc} generated by E-TENG using Ecoflex porous balls as oscillators is 239 V. As can be seen from Fig. 2c(iii and iv), the peak short-circuit current (I_{sc}) generated by CESO as an oscillator is 14.5 μA. The peak I_{sc} generated by E-TENG using Ecoflex porous balls as oscillators is 11.5 μA. As can be seen from Fig. 2c(v and vi), the peak surface charge (Q) generated by CESO as an oscillator is 70 nC. The peak Q generated by E-TENG using Ecoflex porous balls as oscillators is 40 nC. It can be seen that the power generation performance of the TENG is improved after the addition of CNC, and the CESO increases the U_{oc}, the I_{sc} and the Q of the spherical friction nanogenerator by 13.8%, 26% and 75%, respectively (Table S1†). In addition, the charging performance of CNC/E-TENG on capacitors can be seen in Fig. S2.†

The stretchability of the object can reflect its durability. As the friction layer material is more elastic, the as-prepared coconut-derived TENG could withstand more significant mechanical energy input. Moreover, their easy handling, high

mechanical strength, and biodegradable characteristics are the keys to a durable and green energy source for assembling the friction layer of spherical CNC/E-TENG. Thus, we prepared membrane samples and compared their elasticity after CNC was added to them. Fig. 2d shows that the CNC-Ecoflex film was stretched to 212% compared with the Ecoflex film without nanofiber additives (162%), presenting excellent stretchability. The comparison shows that the tensile length of CNC/Ecoflex is 30.7% longer than that of Ecoflex, and the tensile performance of Ecoflex film doped with CNC is better, indicating that the durability of CNC/E-TENG is better.[24]

3.2 Tunable morphology and structure of as-prepared samples

As shown in Fig. 3a–f, both EPPS and LSPS possess hierarchical three-dimensional (3D) porous structures, in which the micrometer-scale pores were not affected by the modification process. The 3D and porous structure of the sponge was not destroyed by the modification process. By observing the SEM images on the surface of LSPS (Fig. 3f), the cluster structure of lignin/SiO$_2$, which is absent on the surface of EPPS (Fig. 3c), was found. The cluster is crucial for improving the lipophilic hydrophobicity of sponges. The unique microstructure of the LSPS makes the skeleton of the sponge rougher, but the pores inside the sponge are not clogged. It is suggested that the lignin/SiO$_2$ composites adhere to the sponge skeleton through the van Der Waals force[25] interaction between lignin/SiO$_2$ and the sponge, resulting in the increase of the surface roughness of the skeleton. The three-dimensional (3D) structure (Fig. 3e) and rough skeleton surface (Fig. 3f) together contribute to the LSPS's strong hydrophobic-ultra-lipophilic and good storage space for oil contaminants. In addition, the presence of SiO$_2$ in the LSPS sample was confirmed by elemental EDS analysis (Fig. S3†).

In the SEM images (Fig. 3g–i), a cluster structure of CNC was observed on the silicon surface, which is essential to improving friction's surface roughness and electronegativity.

The chemical elements of lignin are mainly hydrogen and oxygen, which overlap with the elements of silicone rubber. Thus, the lignin as a crystal was determined by XRD and FTIR in Fig. 3j and k. Fig. 3j shows the X-ray powder diffraction (XRD) pattern of LSPS, EPPS and EPSS samples. It can be seen that there is a strong diffraction peak of the crystal face of pure lingin at approximately $2\theta = 13°$. Although LSPS has more significant variation than a crystalline system, the presence of different chemical species, such as Si–O and Si–OH, characteristic of a silica system, can be determined.

In order to evaluate the chemical structure of Eco/SiO$_2$/lignin hybrid materials (EPPS, EPSS, and LSPS), their FTIR spectra are displayed in Fig. 3k. For the porous silicone foam (EPPS), NH$_2$ twisting vibration was possible at 907 cm^{-1} was detected for both 3D porous PDMS and silicone rubber foam. This peak can be ascribed to a small amount of residual non-cross-linked curing agent entrapped in the framework.[26] The peaks at 1208 cm^{-1}, 1259 cm^{-1}, and 1343 cm^{-1} were assigned to the C–H bond (–CH$_2$, –CH$_3$) stretching vibrations of the polymer chain, while the C–O stretching vibration was observed at 1036 cm^{-1}

and 988 cm^{-1}. It was assigned to the C=O stretching vibrations. According to the spectrum of EPSS, the typical absorption peaks at 1258 cm^{-1} (Si–CH$_3$), 1008 cm^{-1} (Si–O–Si), and 803 cm^{-1} (CH$_3$–Si) could confirm that the PDMS chain segment has been successfully introduced into the surface of SiO$_2$.[27] After lignin addition, it was found that the FTIR bands had altered. The CH$_2$ group at 2962 cm^{-1} may be antisymmetric stretching vibration (CH$_2$ group is connected with N atom, and the frequency of CH$_2$ stretching vibration shifts to high frequency due to the hyper-conjugation effect). Thus, these are vibrations within the biphenyl ring of lignin in LSPS, which were slightly shifted compared to the antisymmetric stretching vibrations of the phenyl ring in EPSS and EPPS. Surely, not all bands of lignin and SiO$_2$ are visible in the spectra of the investigated mixtures as they are overlapped by the bands connected to the main component—silicone rubber substrate. Importantly, the bands connected to lignin, which were visible in the spectra of hybrid materials, were at exactly the same wavenumbers as in the spectrum of EPSS and EPPS. This means that the addition of lignin in LSPS does not change the chemical bonding in the hybrid materials. Compositional analysis and distribution spectrum diagram of LSPS is provided in the ESI (Fig. S4).†

Fig. 4a(i) shows the water contact angle (WCA) of the EPPS produced by the above method within 0–10 minutes. The WCA is 119° at 0 s. The unmodified sponge already shows certain hydrophobicity. Fig. 4a(ii) shows the WCA within 0–10 minutes of the modified EPPS that has not been immersed in the modified lignin clear liquid (*i.e.*, solution A of Fig. 1d) and has been directly immersed in the uniform mixture of petroleum ether and SiO$_2$ (*i.e.*, solution B of Fig. 1d). The WCA of EPSS has been significantly improved, and the WCA increases from 119° to 130° at 0 s. Fig. 4(iii) shows the picture of 0–10 minutes WCA of the LSPS produced in the final paper. The WCA of the LSPS was as high as 150° at 0 s, which was 29° higher than EPPS and was 18° higher than EPSS. LSPS is rougher than the surface of most silicone sponges and has a larger surface WCA. After 10 minutes, the WCA of the LSPS was 138°, which still maintained strong hydrophobicity. When the concentration of SiO$_2$ was increased to twice the original, the WCA of LSPS reached 150°, and it was successfully modified into a superhydrophobic material (Fig. 4a(iii)). The above shows that proper addition or increase of the concentration of modified lignin molecules and SiO$_2$ can improve the hydrophobicity of sponges. Fig. 4b shows the picture of oil contact angle (OCA) of LSPS. It can be seen that oil droplets were immersed into the sponge quickly and easily, and the OCA was 0°.

Fig. 4c shows the states of various oils and water on the surface of LSPS. The four selected oils are as follows: silicone oil, *n*-heptane, pump oil and soybean oil can be soaked in LSPS, and water droplets can be spherical on the surface of LSPS. As shown in Fig. 4d, when the LSPS is immersed in water through external force, a mirrorlike surface is formed on the LSPS due to the interface formed between the trapped air in the sponge and the surrounding water. This phenomenon can use Cassie–Baxter[28] of wetting behavior to explain, illustrates the LSPS on the water from the non-invasive, namely hydrophobic. The
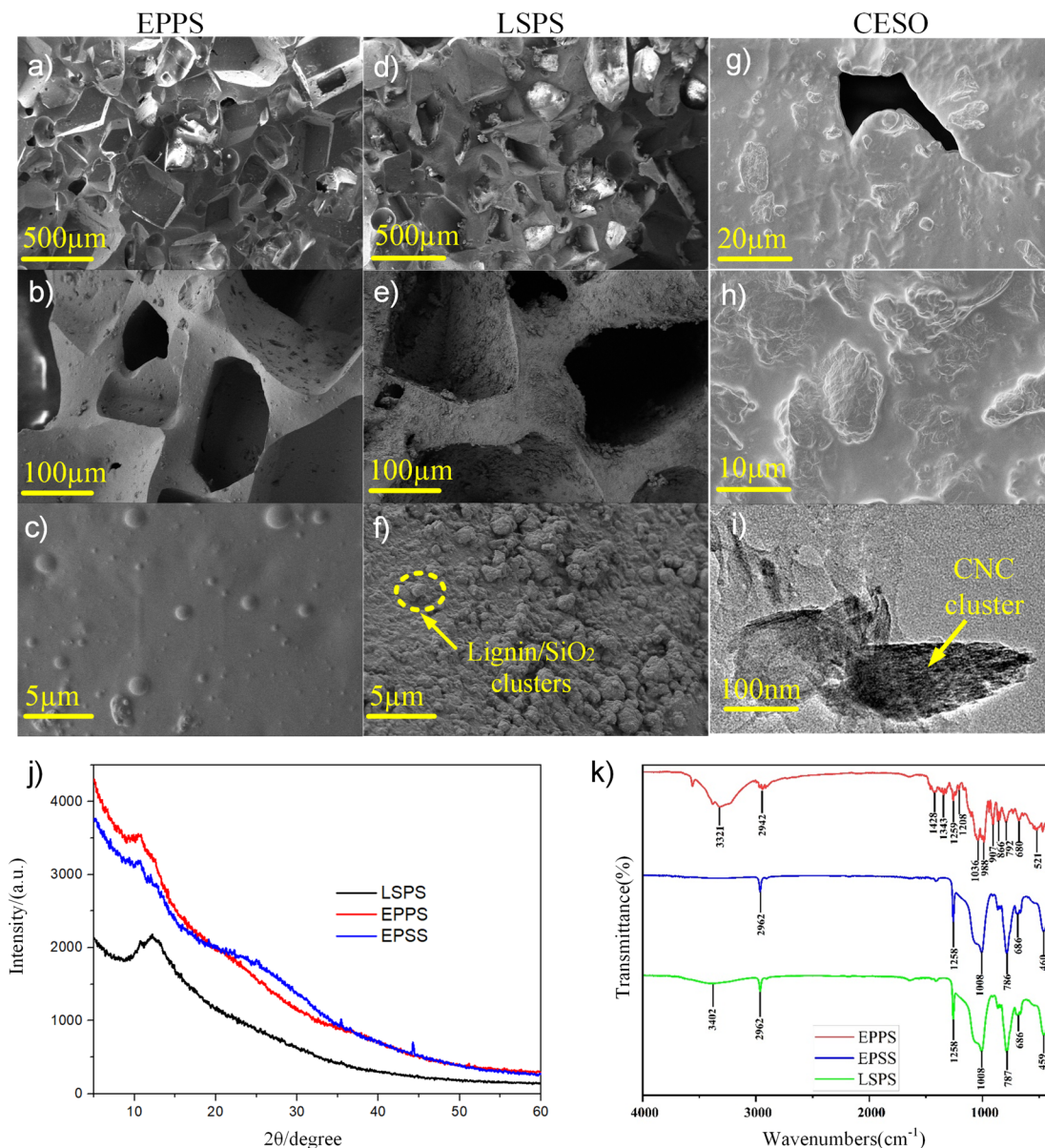
Fig. 3 (a–i) SEM images of EPPS, LSPS and CESO. (j) The X-ray powder diffraction (XRD) pattern of LSPS, EPPS and EPSS samples. (k) FTIR spectra of the as-fabricated EPPS, EPSS, and the composite LSPS with 10.3 wt% of lignin.

results show that the LSPS has super lipophilicity and strong hydrophobicity.

The axial compression experiment of LSPS with a density of 7.58 mg cm^{-3} was measured with 50% strain (Fig. 5a). The stress–strain curve revealed its good rebound resilience with cycle compression. The non-linear elasticity occurs in LSPS as a result of the chain segment and phase structure of the lignin hybrid silicone, and the LSPS sample reached a maximum compressive strength of 11.42 kPa.

The oil absorption rate of the sponge decreases with the increase of oil viscosity. This was due to when the viscosity of oil increases, the mutual attraction between oil molecules becomes stronger, and it is easier to form solidified clumps on the surface of the sponge, making it more difficult for oil molecules

to enter the pores of the sponge. Oil porous with low viscosity can significantly change the state of sponges and has been stored in large quantities in the sponges (Fig. S5†).

It can be seen from Fig. 5b that the oil absorption rate of lignin/SiO$_2$ porous sponge on three kinds of oil is higher than that of the other two sponges, which is due to the oleophilic properties of lignin molecules in lignin/SiO$_2$ porous sponge. The capillaries of the superhydrophilic microtubules are perceived to drive the oil into the pores of the sponge. A large number of lignin/SiO$_2$ clusters are distributed on the surface of LSPS, which improves the surface roughness of LSPS, and then improves the oil absorption ability of LSPS. The oil absorption ratio to *n*-heptane was 4.5 g g^{-1} (Fig. S5†). As shown in the inner inset of Fig. 5b, the LSPS can obtain the oil stored in the sponge
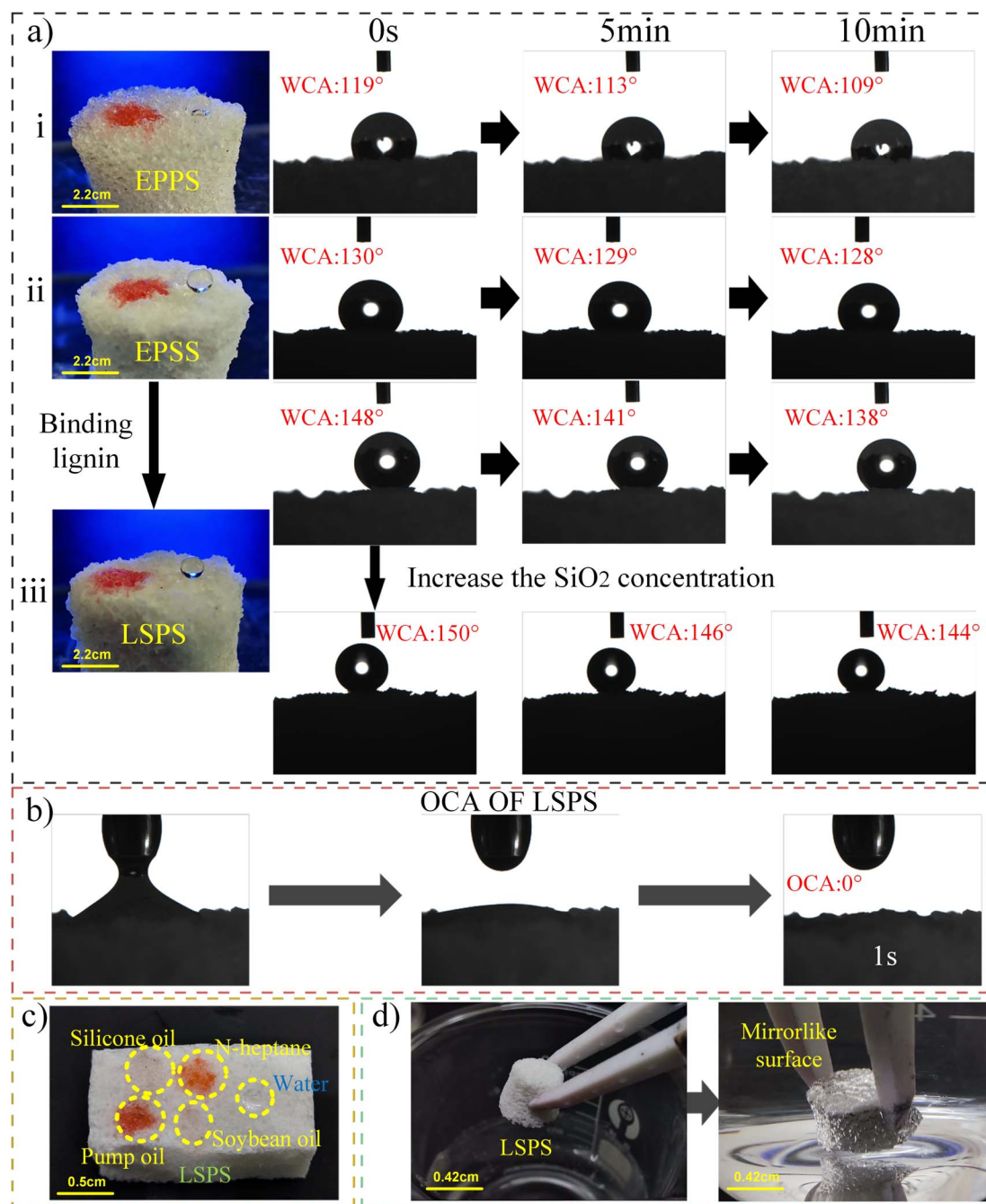
Fig. 4 (a) Photo of water contact angle. (b) Photo of oil contact angle of LSPS. (c) Photographs of various oils and water on the surface of LSPS. (d) The phenomenon of LSPS in water.

by extrusion after oil absorption, making the process of oil recovery easier, faster and more adequate (Fig. S6†).

As shown in Fig. 5c, the whole process of static selective oil absorption experiment is shown. It is concluded that LSPS has superoleophilic and strong hydrophobicity, and has good selective adsorption properties for oil dirt in oil–water mixture. When LSPS was in contact with *n*-heptane (stained red by Sudan Red II (AR)) on the surface of deionized water, it was able to absorb oil layer relatively quickly while rejecting water layer. Due to its low density, LSPS was able to absorb oil layer relatively

quickly. It is hydrophobic and can float on water Fig. 5c. Because the LSPS lacks magnetism, the oil can be completely removed manually, as shown in (Video S1†).

As shown in Fig. 6a, in order to study the continuous selective adsorption properties of LSPS under dynamic conditions, an oil–water separation device combined with a peristaltic pump was prepared for dynamic pumping adsorption experiment. A magnetic stir bar was used to stir the water to mimic ocean conditions, stirring it into a rotating vortex with bubbles flowing upward (Fig. 6a). As shown in Fig. 6a, the results show
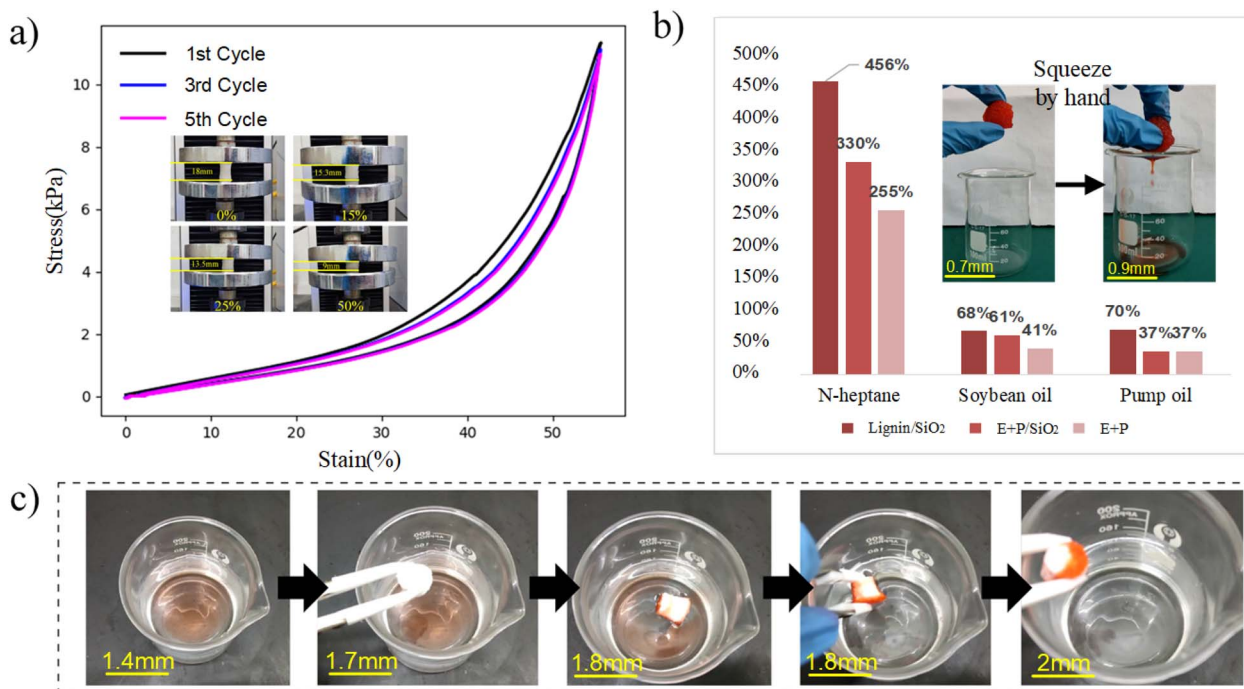
Fig. 5   (a) The compressibility of LSPS. (b) The oil absorption rate of three kinds of sponges absorbing three kinds of oil and recycling methods. (c) Removal of n-heptane stained by Sudan Red II (AR) in water.

that the system can perform continuous selective adsorption and oil–water separation. When the LSPS is placed at the oil–water interface, it rapidly absorbs oil and completely repels water due to its ultra-oleophilic and strong hydrophobicity. Once the peristaltic pump is turned on and the pressure drive system works, the capillary action and selective absorption of the LSPS combine to pump oil rapidly upward through the pipeline. Furthermore, oil absorbed by the sponge has been transferred into the empty beaker through the action of negative pressure for oil collection and storage. Oil flows in the pipeline and the thickness of the reservoir gradually decreases (Fig. 6a). Finally, by close-up of the beaker on the left, it is found that there is no significant change in the water level, and the oil layer floating on the water surface completely disappears, which can be considered that the device successfully collected all the oil on the water surface (Fig. 6a), as shown in (Fig. S7†). Moreover, LSPS combined with a Peristaltic pump can complete the oil–water separation of 20 ml n-heptane within 70 s (Video S2†). It is sufficient to prove that LSPS has strong continuous oil–water separation ability.

As shown in Fig. 6b, after 100 static oil absorption cycles, the absorption capacity of LSPS increased slightly, which may be related to the fragile adhesion-modified lignin on the LSPS skeleton.[29] Another reason may be that the mass of LSPS decreases with the number of static cycle experiments, resulting in a slight increase in absorption. The results show that LSPS has good recyclability and durability.

As shown in Fig. 6c, the oil–water separation rate of LSPS remained near 95% after 20 cycles, indicating that LSPS had good recyclability. At the maximum power, the oil dialysis capacity remained near 33970 L m^{-2} h^{-1} (the oil and water separation of 20 ml n-heptane can be performed for an average of 75 s at full power), indicating that LSPS had stable oil dialysis capacity under different cycles. The results show that LSPS has good recyclability and durability.

3.3   Nanofiber enhanced marine self-healing system based on biomass structure

Eventually, to gain an overall insight into the mechanism of the marine self-healing system, the typical diagram of spilling oil pollution treatment with a self-powering peristaltic pump and oil–water separation material (LSPS) was demonstrated in Fig. 6d. One of the keys to improving the system's performance is to increase the hydrophobicity of the material, which is mainly dependent on the surface topography of the porous sponges. We also compared the WCA and parameters of other biomass-based oil/water-separating materials (Table S2†). Due to the high adhesion energy, which was responsible for the larger contact angle of LSPS than other materials, which can further guide the design of biomimetic superhydrophobic surfaces and the excellent wetting behavior. Meanwhile, based on the internal porous structure and the presence of SiO$_2$ on the sponge skeleton, the water droplet can be expected to partially permeate into the pores of LSPS without immediate contact, leading to the unusual Cassie impregnating wetting state as illustrated in Fig. 6e. On the other side, the continuous and stable operation of the system requires the high charge density of TENG. Fig. 6f shows a schematic illustration of an electron potential well model of the difference between biomass-based coconut shell and nanofiber-enhanced CESO with CNC. Due
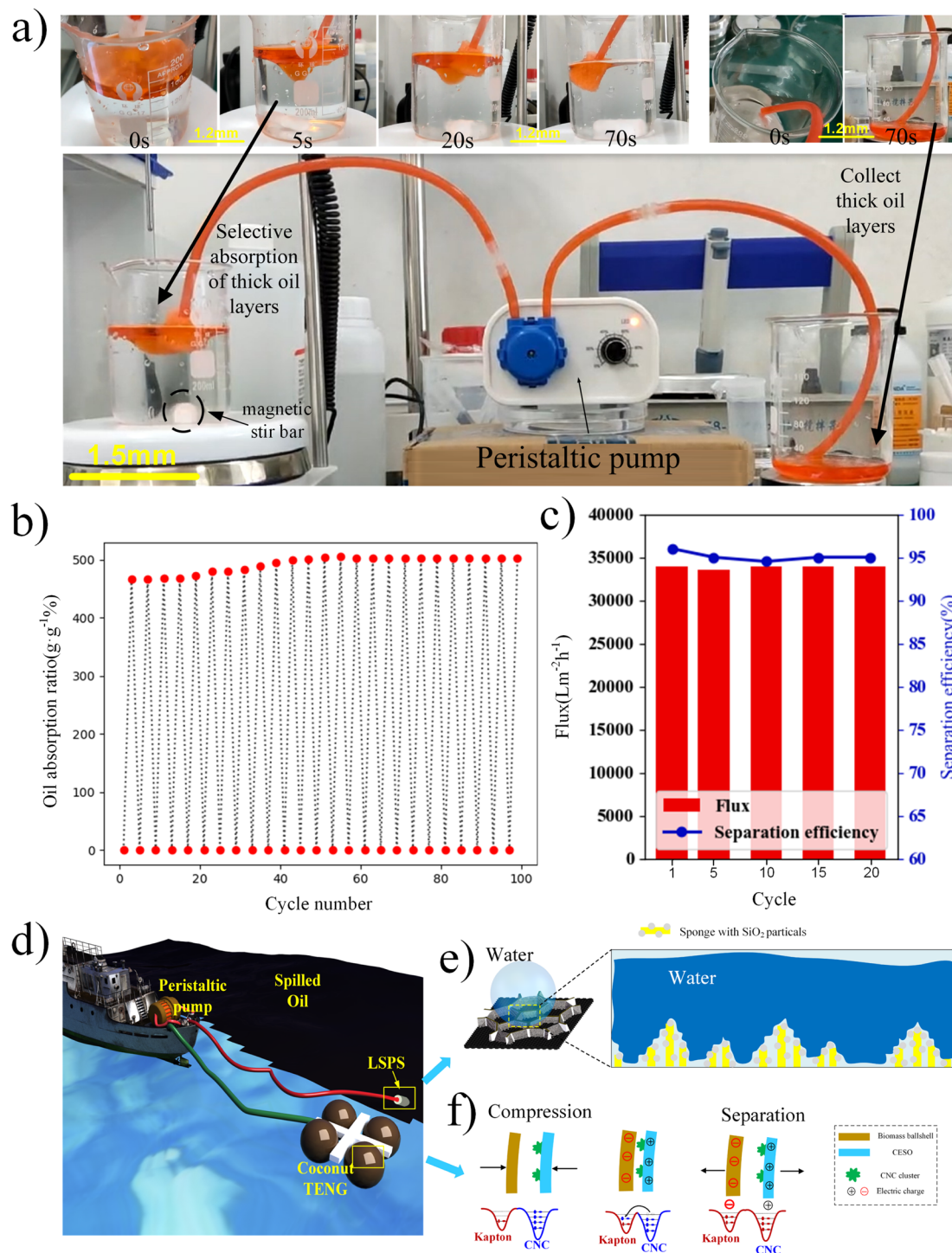
Fig. 6 (a) Oil absorption experiments with LSPS combined with peristaltic pump. (b) Static oil suction cycle. (c) Dynamic oil–water separation cycle. (d) The typical diagram of spilling oil pollution treatment with a self-powering peristaltic pump and oil–water separation material (LSPS). (e) Mechanism of enhancing hydrophobicity of porous sponges by nanofibers. (f) Mechanism of enhancing electrical properties of TENG by nanofibers.

to the high escaping energy barrier, their electrons are tightly confined in their original orbits before contact. With the kinetic energy provided by the wave to the oscillator, the surfaces of the two layers are compressed against each other. As their electron clouds overlap strongly in contact, the Triboelectric effect

significantly reduces the interatomic potential barrier (Fig. 6f). Finally, some high-energy electrons in the nanocellulose can easily overcome the reduced potential barrier and transfer to the Kapton to achieve equilibrium. After the two materials are separated, the transferred electrons and holes remain static

charges on the CNC and coconut shell surfaces, respectively. Thus, the combination of nanocellulose-based polymer hybrid and biomass-based modified strategy provides a novel idea for the sustainable and efficient operation of a self-powering oil–water separation system.

4 Conclusion

In summary, the coconut husk-derived and coir fiber-reinforced biocomposites with high sorption capacity and excellent triboelectricity were successfully prepared *via* a promising synthetic strategy. The Coir lignin hybridized LSPS, with superhydrophobicity (WCA = 150°) and facile recyclability, accomplished the continuous selective separation of oil/water mixtures under pumping action. Furthermore, the LSPS accomplished the continuous selective separation of oil/water mixtures under pumping action. Notably, the nanofiber-modified CESO assembled with degradable coconut husk could output the cyclic periodic electrical signal under low frequency with external mechanical excitations. The combination of nanocellulose-based polymer hybrid and biomass-based modified strategies provides a novel idea for the sustainable and efficient operation of a self-powering oil–water separation system.

Conflicts of interest

The authors declare no competing financial interest.

Acknowledgements

References

1 R. A. Magris and T. Giarrizzo, *Mar. Pollut. Bull.*, 2020, **153**, 110961.

2 J. Li, *Compensation for Damage to Marine Biodiversity under International Liability Regime on Vessel-Source Marine Oil Pollution Damage*, 2015.

3 Y. Guan, F. Cheng and Z. Pan, *Polymers*, 2019, **11**, 806.

4 Y. Luo, S. Jiang, Q. Xiao, C. Chen and B. Li, *Sci. Rep.*, 2017, **7**, 7162.

5 W.-Y. Zhu, X. Zhao and Y.-C. Hu, *Xiandai Huagong*, 2018, **38**, 96–100.

6 L. Passauer, T. Hallas, E. Baucker, G. Ciesielski, S. Lebioda and U. Hamer, *ACS Sustain. Chem. Eng.*, 2015, **3**, 1955–1964.

7 J. Guo, W. Fang, A. Welle, W. Feng, I. Filpponen, O. J. Rojas and P. A. Levkin, *ACS Appl. Mater. Interfaces*, 2016, **8**, 34115–34122.

8 H. Sun, Z. Liu, K. Liu, M. E. Gibril, F. Kong and S. Wang, *Ind. Crops Prod.*, 2021, **170**, 113798.

9 F. Monteil-Rivera, M. Phuong, M. Ye, A. Halasz and J. Hawari, *Ind. Crops Prod.*, 2013, **41**, 356–364.

10 Y. Meng, T. Liu, S. Yu, Y. Cheng, J. Lu and H. Wang, *Fuel*, 2020, **278**, 118376.

11 S. Song, H. Yang, C. Su, Z. Jiang and Z. Lu, *Chem. Eng. J.*, 2016, **306**, 504–511.

12 H. Yang, X. Hu, R. Chen, S. Liu, P. Pi and Z. ru Yang, *Appl. Surf. Sci.*, 2013, **280**, 113–116.

13 J. Li, R. Kang, X. Tang, H. She, Y. Yang and F. Zha, *Nanoscale*, 2016, **8**, 7638–7645.

14 L. Wu, L. Li, B. Li, J. Zhang and A. Wang, *ACS Appl. Mater. Interfaces*, 2015, **7**, 4936–4946.

15 X. Gong, Y. Meng, J. Zhu, X. Wang, J. Lu, Y. Cheng, Y. Tao and H. Wang, *Ind. Crops Prod.*, 2021, **166**, 113471.

16 F.-R. Fan, Z.-Q. Tian and Z. L. Wang, *Nano energy*, 2012, **1**, 328–334.

17 W. Zhang, W. He, S. Dai, F. Ma, P. Lin, J. Sun, L. Dong and C. Hu, *Nano Energy*, 2023, **111**, 108432.

18 Y. Li, Z. Guo, Z. Zhao, Y. Gao, P. Yang, W. Qiao, L. Zhou, J. Wang and Z. Wang, *Appl. Energy*, 2023, **336**, 120792.

19 M. Gao, Z. Chen, J. Liang, Z. Lin, Y. Zhou, J. Li, G. Li, L. Mo, J. Shao and Y. Luo, *ACS Appl. Polym. Mater.*, 2023, **5**, 5074–5081.

20 S. Liu, X. Liang, P. Chen, H. Long, T. Jiang and Z. L. Wang, *Small Methods*, 2023, **7**, 2201392.

21 B. Nayak, H. Acharya, G. Mitra and B. Mathur, *Thin Solid Films*, 1983, **105**, 17–24.

22 Z. Ye, S. Liao, F. Wang, L. Mo, G. Li and Y. Luo, *IOP Conf. Ser. Earth Environ. Sci.*, 2022, **966**, 012011.

23 Z. Bo, D. Shulin, L. Zihao and Z. Baocheng, *Tribology*, 2020, **40**, 680–686.

24 S. Wang, Q. Zou, L. Zhang, W. Zheng, X. Huang and J. Zhang, *Ind. Crops Prod.*, 2023, **197**, 116607.

25 I. E. Dzyaloshinskii, E. M. Lifshitz and L. P. Pitaevskii, *Soviet Phy.-Uspekhii*, 1961, **4**, 153.

26 J. González-Rivera, R. Iglio, G. Barillaro, C. Duce and M. R. Tinè, *Polymers*, 2018, **10**, 616.

27 L. Jia, J. Sun, X. Li, X. Zhang, L. Chen and X. Tian, *Coatings*, 2021, **11**, 256.

28 L. Wen, Y. Tian and L. Jiang, *Angew. Chem., Int. Ed.*, 2015, **54**, 3387–3399.

29 X. Ma, C. Zhang, P. Gnanasekar, P. Xiao, Q. Luo, S. Li, D. Qin, T. Chen, J. Chen, J. Zhu and N. Yan, *Chem. Eng. J.*, 2021, **415**, 128956.